Joint friction estimation for walking bipeds

Iyad Hashlamon and Kemalettin Erbatur

Robotica / *FirstView* Article / November 2014, pp 1 - 20
DOI: 10.1017/S0263574714002471, Published online: 05 November 2014

Robotica: page 1 of 20. © Cambridge University Press 2014
doi:10.1017/S0263574714002471

Joint friction estimation for walking bipeds

Iyad Hashlamon and Kemalettin Erbatur

Faculty of Engineering and Natural Sciences, Sabanci University, Tuzla, Istanbul, Turkey
E-mail: erbatur@sabanciuniv.edu

(Accepted September 23, 2014)

SUMMARY
This paper proposed a new approach for the joint friction estimation of non-slipping walking biped robots. The proposed approach is based on the combination of a measurement-based strategy and a model-based method. The former is used to estimate the joint friction online when the foot is in contact with the ground, while the latter adopts a friction model to represent the joint friction when the leg is swinging. The measurement-based strategy utilizes the measured ground reaction forces (GRF) and the readings of an inertial measurement unit (IMU) located at the robot body. Based on these measurements, the joint angular accelerations and the body attitude and velocity are estimated. The aforementioned measurements and estimates are used in a reduced dynamical model of the biped. However, when the leg is swinging, this strategy is inapplicable. Therefore, a friction model is adopted. Its parameters are identified adaptively using the estimated online friction whenever the foot is in contact. The estimated joint friction is used in the feedback torque control signal. The proposed approach is validated using the full-dynamics of 12-DOF biped model. By using this approach, the robot center of mass (CoM) position error is reduced by 10% which demonstrates the effectiveness of this approach.

KEYWORDS: Humanoid robot; Joint friction; Non-slipping feet; CoM states; Biped model.

1. Introduction

Humanoids are the most versatile robots employed in the human environment because of their remarkable advantages stemming from their bipedal structure. Humanoids can easily avoid the obstacles via leg-based locomotion capabilities. These enable the bipeds to widely operate in human environments such as offices and factories.[1] Moreover, their high mobility enhances their use in human assisting applications.[2] In the same context, humanoid robots are helpful in replacing humans in hazardous environments.[3]

The research trend of the biped adaptive, efficient and robust walking is highly demanding.[4–11] However, the biped has many coupled degrees of freedom (DOF) to be controlled. Moreover, bipeds are highly nonlinear and complex to be dynamically stabilized. One more difficulty rises from the complexity of the mechanical structure of the robots. In general, the robot mechanical structure contains transmissions or drive mechanisms to transfer the power from the actuator to the robot link through the joint.[12] Therefore, friction is observed at the joints. This friction has a considerable effect on the robot behavior. Joint friction may deteriorate the robot performance resulting in unwanted consequences such as steady state errors, limit cycles and poor responses.[13–15] Therefore, joint friction compensation received a considerable interest in various studies.[16,17] Here, the compensation of the joint friction is divided into three methods: friction model-based, model-free and actuator fault-based. These methods are discussed with their advantages and disadvantages in the next subsection.

1.1. Related work

In the first joint friction compensation method, the friction behavior is based on a mathematical model.[18–21] The model parameters are identified offline. Then the model with the identified parameters

* Corresponding authors. E-mail: hashlamon@sabanciuniv.edu, erbatur@sabanciuniv.edu

is used to compensate for the joint friction.[22–27] However, the friction model parameters vary due to environmental changes like surfaces and wear. Moreover, the friction is a complex phenomenon that depends on factors including joint position and load.[28] To overcome these problems, model-based adaptive methodologies were developed. In these methodologies, the friction model parameters are tuned online to obtain a satisfactory compensation action.[29–33] However, friction modeling is a challenge since the friction behavior is highly nonlinear. Therefore, the tendency is to develop more detailed friction models to evoke the online friction compensation procedure.[21]

The second method is based on a model-free approach. **S**everal strategies are used here to compensate for the friction. One strategy relies on the measurement-based friction compensation.[34,35] The transmitted torque to the manipulator's link is measured by torque sensors and used in the feedback torque control loop. Although the performance of the measurement-based strategy is shown to be effective in practice,[34,35] the torque sensors should be added in the design process. The drawback of mounting extra torque sensors was solved for the fixed base robots by using the base sensor control (BSC) method.[28] The BSC method assumes that the robot base is equipped with a force/torque sensor then it projects the sensor readings on the robot links to compute the manipulator's link torque. This torque is consequently used in the feedback torque control law. However, the biped robot is not fixed to ground.

Another strategy is based on the disturbance observer (DO) theory.[36,37] In this strategy, the friction, external disturbances, system model uncertainty, gravity torque and so on are regarded as sources of disturbance. The DO is used to eliminate the effects of this disturbance based on the frequency band.[38–40] Notably, it is assumed that the observer dynamics are faster than the disturbance. Combining the DO with the model**-**based method is reported to improve the system performance as they complement each other.[41] However, the design of the DO depends on the low pass filter design, and there is no systematical filter design criterion.[38]

Friction approximator is another strategy which uses the soft computing techniques. Neural networks (NNs) are characterized by the parallelism and low level learning. NNs are able to approximate the nonlinear functions. Using this property, NNs are used to build compensators for the friction models.[42–44] NNs are also used to handle the unknown dynamics including friction discontinuity.[30] However, the approximation error exists and depends on the structure of the NN. Heavy computation is the result of an overdetermined NN while low approximation accuracy will be obtained from an underdetermined NN. Furthermore, NNs are locally applicable and sensitive to the NN initialization.[45] In addition**,** fuzzy systems are used for friction approximation. Fuzzy systems are characterized by the linguistic information and the high level of logic. Fuzzy systems are universal approximators for nonlinear functions and functionally equivalent to feed-forward NNs. This property gives them the ability to build models to represent the friction behavior.[46–51] However, the approximation error does also exist.

The third method treats the friction as an actuator fault with time varying characteristics. The friction is compensated based on the robust fault estimation theory. To accomplish this, the fault-tolerant control (FTC) scheme is used for linear systems.[52]

1.2. Problem definition

Joint friction compensation is of great importance. It is studied intensively for the industrial robots. However in bipeds, joint friction compensation is generally neglected.[53–56] The reported studies that considered the joint friction are few. They are either model-based or model-free. In the former method, the friction model with the offline identified parameters is used to compensate for the joint friction.[22,57] **T**he latter regards the joint friction as disturbance, and the DO is used to eliminate it.[38] However, both of them have the aforementioned drawbacks.

Among the model-free strategies, the measurement-based strategy is fruitful. It is the goal for the online friction compensation since it avoids the friction modeling and approximation problems. However, the measurement-based strategy cannot be applied on bipeds if there are no mounted joint torque sensors. Moreover, the bipeds are not fixed to ground. While walking, the biped switches its legs from the double support phase (DS) to the single support phase (SS) and so forth. The model-based method is characterized by having much precision friction compensation if the identified parameters have very small uncertainty.[58] The high accuracy can be achieved by adaptive model parameter tuning. However, adaptive tuning requires information about the friction to update the model parameters.

The biped dynamical model includes the unmeasured body velocity in addition to the joint angles and their derivatives. This adds more challenge to the friction estimation and compensation problem.

Thus, a method that has the advantages of the measurement-based strategy and the adaptive model-based methodology is sought. Moreover, this method must be able to overcome the challenge of the unmeasured variables in the biped dynamical model.

1.3. The proposed method

In this paper, we propose a novel method combining both model-free and model-based compensation methods. More precisely, the measurement-based strategy is combined with the model-based method of compensation. First, the body attitude is estimated by utilizing the IMU readings through a sensor fusion approach. Then the robot body (called base later on) velocity is estimated using the linear inverted pendulum model (LIPM).[59] This model relates the robot base position, velocity and acceleration with the measured GRF. Bearing in mind the non-slipping foot assumption, the joints accelerations are estimated using the pseudo inverse matrix multiplication.

The measurement-based strategy only functions when the foot is in contact with the ground without slipping. This strategy is employed for two purposes. The first purpose is to provide online feedback joint friction compensation. The joint friction is estimated by using the robot link torque and the applied joint control torque. The robot link torque is computed (not measured) using a reduced dynamical model of the biped. This reduced model utilizes the GRF and the IMU readings. It also utilizes the estimated base velocity and attitude and joints accelerations. However, when the foot loses the contact with the ground, the online friction compensation is no longer applicable. For this case, a friction model is adopted. The second purpose of the measurement-based strategy is to update the adopted friction model parameters. Thus, the model parameters are adaptively identified whenever the foot is in contact with the ground. Hence, the proposed method is measurement-based online friction compensation when the foot is in contact with the ground and model-based adaptive method when the leg is swinging. The proposed method while exploiting the advantages of the measurement-based strategy and the model-based method does overcome their disadvantages. Since this method uses the foot and base measurements it is called: foot base sensor estimation (FBSE).

The rest of the paper is organized as follows: Section 2 describes the biped model. Section 3 introduces the base attitude estimation approach. The base states observer is in Section 4. Section 5 introduces the link torque computation. Section 6 introduces the friction parameter identification and Section 7 presents the results. The paper conclusion is in Section 8.

2. Biped Model

The biped consists of a body and two legs connected to it as in Fig. 1. The biped motion is defined in the fixed world frame O_w. The body is considered as the base link with the base coordinate system O_b. The hips and feet soles have coordinate frames too.

For this work, it is assumed that the biped is equipped with contact force sensors with frame origin O_F assembled at the feet soles,[7] joint encoders attached to the joint actuators and an IMU with a frame origin O_I. The IMU is composed of 3-axes accelerometer and 3-axes gyroscope.

The walking biped is modeled as a free-fall manipulator. For a biped with N joints, and the defined generalized coordinates

$$\mathbf{x}^T = [\mathbf{p}_b^T, \mathbf{A}_b^T, \boldsymbol{\theta}^T] \in R^3 \times SO(3) \times R^N, \tag{1}$$

generalized velocities

$$\mathbf{v}^T = [\mathbf{v}_b^T, \boldsymbol{\omega}_b^T, \boldsymbol{\omega}^T] \in R^3 \times R^3 \times R^N, \tag{2}$$

and generalized forces

$$\mathbf{u}^T = [\mathbf{f}_b^T, \mathbf{n}_b^T, \tau^T] \in R^3 \times R^3 \times R^N, \tag{3}$$

the robot dynamical model is

$$\mathbf{H}(\mathbf{x})\dot{\mathbf{v}} + \mathbf{C}(\mathbf{x}, \mathbf{v})\mathbf{v} + \mathbf{g}(\mathbf{x}) + \mathbf{u_F} = \mathbf{u} + \mathbf{u_E}, \tag{4}$$

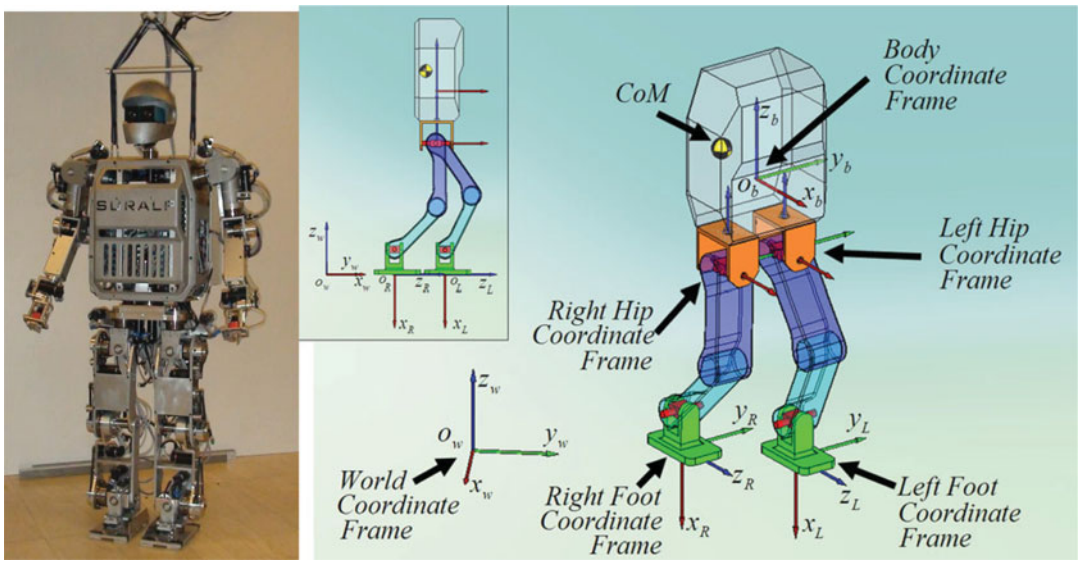

Fig. 1. (Colour online) Left: the humanoid SURALP (Sabanci University Robotics Research Laboratory Platform).[60] Right: coordinate systems. O_w and O_b stand for the origins of the world and body coordinate frames, respectively. The feet coordinate frames are fixed to the feet soles.[8]

where $\boldsymbol{\theta} \in R^N$ is the joint displacements vector and $\dot{\boldsymbol{\theta}} = \boldsymbol{\omega} \in R^N$ the joint angular velocity vector, $\mathbf{A}_b \in SO(3)$ the transformation matrix giving the position of joint axes relative to the world axes, $\mathbf{p}_b$ and $\dot{\mathbf{p}}_b = \mathbf{v}_b$ the position and linear velocity of the base coordinate frame origin, $\boldsymbol{\omega}_b$ the angular velocity of the base coordinate frame and follows the relation $\dot{\mathbf{A}}_b = \boldsymbol{\omega}_b \times \mathbf{A}_b$, $\mathbf{f}_b \in R^3$ the force vector generated in the base, $\mathbf{n}_b \in R^3$ the torque vector generated at base, $\boldsymbol{\tau}$ the generalized joint control vector, $\mathbf{u_F}$ the joint frictional forces vector, the matrix H represents the inertia, the $\mathbf{C}(\mathbf{x}, \mathbf{v})$ matrix specifies the centrifugal and Coriolis effects and the $\mathbf{g}(\mathbf{x})$ vector specifies the gravity effect.

The core of this paper is to estimate the joint frictional forces, so that for simplification, the bias term $\mathbf{b}$ is used as $\mathbf{b} = \mathbf{C}(\mathbf{x}, \mathbf{v})\mathbf{v} + \mathbf{g}(\mathbf{x})$. Then Eq. (4) is rewritten as

$$\mathbf{H}\begin{pmatrix} \dot{\mathbf{v}}_b \\ \dot{\boldsymbol{\omega}}_b \\ \ddot{\boldsymbol{\theta}}_\mathbf{L} \\ \ddot{\boldsymbol{\theta}}_\mathbf{R} \end{pmatrix} + \begin{pmatrix} \mathbf{b_1} \\ \mathbf{b_2} \\ \mathbf{b_L} \\ \mathbf{b_R} \end{pmatrix} + \begin{pmatrix} \mathbf{u}_{\mathbf{F}_1} \\ \mathbf{u}_{\mathbf{F}_2} \\ \mathbf{u}_{\mathbf{F}_\mathbf{L}} \\ \mathbf{u}_{\mathbf{F}_\mathbf{R}} \end{pmatrix} = \begin{pmatrix} \mathbf{f}_b \\ \mathbf{n}_b \\ \tau_\mathbf{L} \\ \tau_\mathbf{R} \end{pmatrix} + \begin{pmatrix} \mathbf{u}_{\mathbf{E}_1} \\ \mathbf{u}_{\mathbf{E}_2} \\ \mathbf{u}_{\mathbf{E}_\mathbf{L}} \\ \mathbf{u}_{\mathbf{E}_\mathbf{R}} \end{pmatrix}, \tag{5}$$

with

$$\mathbf{H} = \begin{pmatrix} H_{11} & H_{12} & H_{13} & H_{14} \\ H_{21} & H_{22} & H_{23} & H_{24} \\ H_{31} & H_{32} & H_{33} & 0 \\ H_{41} & H_{42} & 0 & H_{44} \end{pmatrix},$$

where H_{ij} for $(i, j) \in \{1, 2, 3, 4\}$ are sub-matrices of the robot inertia matrix, $\mathbf{u}_{\mathbf{E}_1}$ the net force effect and $\mathbf{u}_{\mathbf{E}_2}$ the net torque effect of the reaction forces on the base, $\mathbf{u}_{\mathbf{E}_\mathbf{L}}$ and $\mathbf{u}_{\mathbf{E}_\mathbf{R}}$ stand for the effect of reaction forces generated by environmental interaction on the robot joints for the left and right legs, respectively. The subscripts $()_\mathbf{L}$ and $()_\mathbf{R}$ stand for the left and right legs, respectively.

The bipeds are not fixed to the ground, while walking they are switching from the DS phase to the SS phase and so forth. The robot dynamics depend on the attitude $\mathbf{A}_b$ and base velocity $\mathbf{v}_b$. This necessitates looking for a method to estimate $\mathbf{A}_b$ and $\mathbf{v}_b$ based on fussing the readings of the available sensors. Moreover, this estimation must not depend on the biped phase.

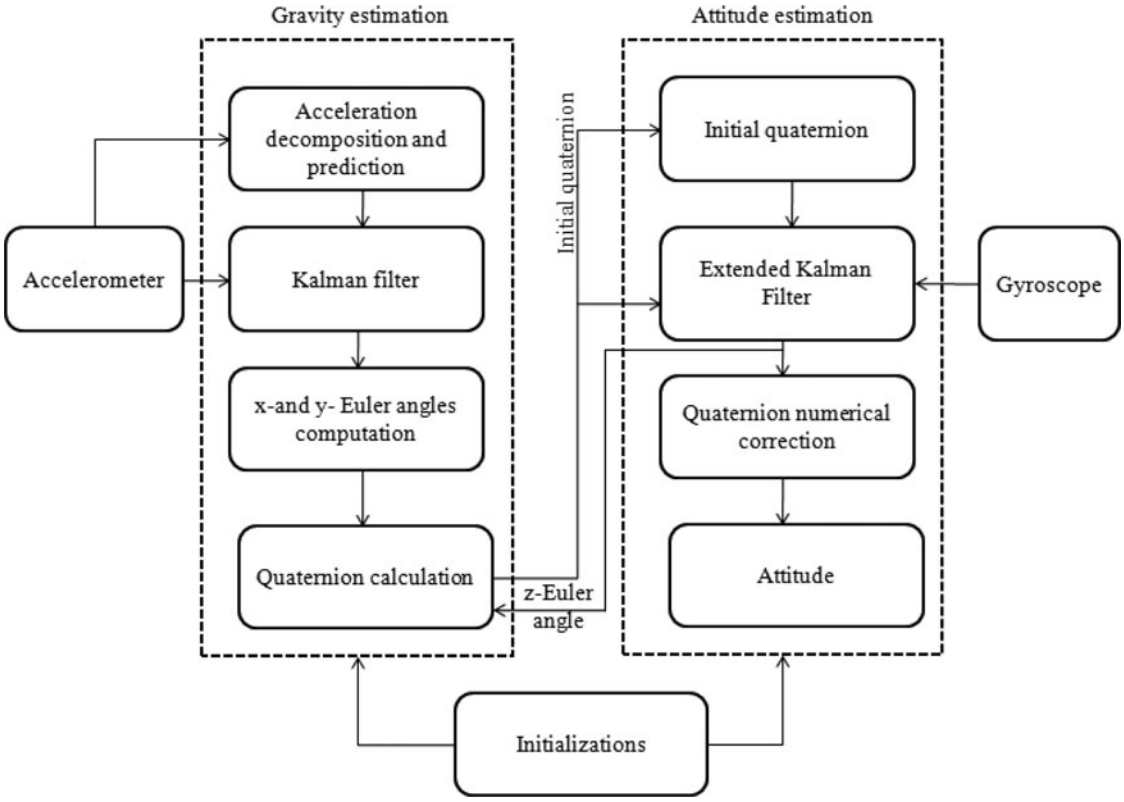

Fig. 2. Attitude estimation approach.

3. Base Attitude Estimation

The authors developed a sensor fusion approach to estimate the attitude of robots by utilizing the IMU readings.[61] This approach is independent on the robot model so that it can be applied for the bipeds too. It employs two sequential estimators. The first estimator is for the gravity estimation and uses Kalman filter (KF). The second estimator is for the attitude estimation and uses the extended Kalman filter (EKF) as in Fig. 2.

KF is employed for the gravity estimation mainly based on acceleration readings. KF states are the gravity acceleration, linear acceleration and acceleration bias. The accelerometer output consists of the gravity acceleration, linear acceleration, bias and noise. The gravity acceleration vector contains information about the roll and pitch angles of the body. To initialize KF states, the accelerometer output signal has to be decomposed. By ignoring the noise, the values of the accelerometer signal terms are predicted using the pseudo inverse matrix multiplication. The predicted values are used as initial values for KF. The gravity acceleration estimate from KF is used for the computation of the x- and y-Euler angles. The computed Euler angles are transformed into quaternion representation to be considered as a "measured quaternion" for the correction stage in the EKF. To accomplish this transformation, the z-Euler angle is also required. The z-Euler angle is borrowed from the quaternion estimate of the EKF and initially it is considered to be zero.

The EKF uses the measured quaternion and the gyroscope readings to produce the correct quaternion vector. Since the quaternion has the unity norm constraint, this correction is followed by a numerical norm correction to keep the unity magnitude of the quaternion. Then the normalized estimated quaternion is converted to represent the attitude. The two estimators feed each other cyclically: The EKF provides the z-Euler angle for the gravity estimator, whereas the gravity estimator produces the measured quaternion for the attitude estimator. The noise covariances initializations are provided for both estimators.

The resulted attitude matrix A_I^w represents the attitude of the IMU frame O_I with respect to O_w. It is assumed that the IMU is fixed at a known position r_I and attitude A_I^b with respect to O_b. Thus,

the base frame attitude $\mathbf{A}_b$ with respect to O_w can be calculated as

$$\mathbf{A}_b = A_I^w A_b^I. \tag{6}$$

A_b^I is the rotation of O_b frame with respect to O_I frame. The rotation matrices have the properties $A_b^I = (A_I^b)^T = (A_I^b)^{-1}$ since the coordinate system is orthogonal.

4. Base States Observer

The base velocity and acceleration states have an important role in the estimation process. The acceleration is measured, however the velocity is not. A sensor fusion approach is used here to estimate the base velocity by utilizing the GRF and IMU readings into the LIPM. In this model, the base is modeled as a point mass concentrated at the CoM. This mass is connected to a stable contact point on the ground using a massless rod.[62] The CoM has fixed height z_c and position coordinates in the three dimensional space $\mathbf{c} = [\, c_x \;\; c_y \;\; z_c \,]^T$. The LIPM is given by

$$\ddot{\mathbf{c}} = \frac{g}{z_c}\left(\mathbf{c} - \mathbf{p_{ZMP}}\right), \tag{7}$$

where g is the constant gravity acceleration, $\mathbf{p_{ZMP}}$ the zero moment point[63,64] and $\ddot{\mathbf{c}}$ the CoM acceleration. The model (7) requires the $\mathbf{p_{ZMP}}$ which can be calculated using the feet contact force measurements $\mathbf{F_E}$ to form $\mathbf{p}_{\mathbf{ZMP}}^{\mathbf{F_E}}$ as[65]

$$\mathbf{p}_{\mathbf{ZMP}}^{\mathbf{F_E}} = \frac{\boldsymbol{\rho}_{\mathbf{L}}\left(\mathbf{F}_{\mathbf{E,L}} \cdot \hat{z}_w\right) + \boldsymbol{\rho}_{\mathbf{R}}\left(\mathbf{F}_{\mathbf{E,R}} \cdot \hat{z}_w\right)}{\left(\mathbf{F}_{\mathbf{E,L}} \cdot \hat{z}_w\right) + \left(\mathbf{F}_{\mathbf{E,R}} \cdot \hat{z}_w\right)}, \hat{z}_w = \begin{bmatrix} 0 & 0 & 1 \end{bmatrix}^T, \tag{8}$$

where

$$\boldsymbol{\rho}_{\mathbf{m}} = \left(\mathbf{p_m} + \mathbf{p}_{\mathbf{m,CoP}}\right), \tag{9}$$

and

$$\mathbf{m} = \begin{cases} \mathbf{L} & \text{left leg} \\ \mathbf{R} & \text{right leg} \end{cases}. \tag{10}$$

Here, $\mathbf{p}_{\mathbf{m,CoP}}$ is the position of the center of pressure (CoP) for the foot $\mathbf{m}$, $\mathbf{F}_{\mathbf{E,R}}$ and $\mathbf{F}_{\mathbf{E,L}}$ the force vectors measured from the contact force sensors, $(\mathbf{F}_{\mathbf{E,m}} \cdot \hat{z}_w)$ the dot product and $\mathbf{p_m}$ the position of the foot frame origin for the leg $\mathbf{m}$, it is given by the forward kinematics as $\mathbf{p_m} = f_{\mathbf{m}}(\mathbf{x})$.

The LIPM (7) can be written in several discrete state space models depending on the considered states, inputs and measurements.[66–68] Let $(\,\mathbf{c}^T \;\; \dot{\mathbf{c}}^T \;\; \ddot{\mathbf{c}}^T\,)^T$ be the states. With this state description, Eq. (7) can be written[66] as

$$\frac{d}{dt}\begin{bmatrix} \mathbf{c} \\ \dot{\mathbf{c}} \\ \ddot{\mathbf{c}} \end{bmatrix} = \begin{bmatrix} 0_3 & I_3 & 0_3 \\ 0_3 & 0_3 & I_3 \\ 0_3 & 0_3 & 0_3 \end{bmatrix}\begin{bmatrix} \mathbf{c} \\ \dot{\mathbf{c}} \\ \ddot{\mathbf{c}} \end{bmatrix} + \begin{bmatrix} 0_3 \\ 0_3 \\ I_3 \end{bmatrix}\ddot{\mathbf{c}} \tag{11}$$

$$\mathbf{p_{ZMP}} = \begin{bmatrix} I_3 & 0_3 & -\frac{z_c}{g} I_3 \end{bmatrix}\begin{bmatrix} \mathbf{c} \\ \dot{\mathbf{c}} \\ \ddot{\mathbf{c}} \end{bmatrix}. \tag{12}$$

In discrete from, Eqs. (11) and (12) correspond to

$$\begin{bmatrix} \mathbf{c} \\ \dot{\mathbf{c}} \\ \ddot{\mathbf{c}} \end{bmatrix}_k = \underbrace{\begin{bmatrix} I_3 & I_3 T & I_3 0.5T^2 \\ 0_3 & I_3 & I_3 T \\ 0_3 & 0_3 & I_3 \end{bmatrix}}_{A} \begin{bmatrix} \mathbf{c} \\ \dot{\mathbf{c}} \\ \ddot{\mathbf{c}} \end{bmatrix}_{k-1} + \underbrace{\begin{bmatrix} 0_3 \\ 0_3 \\ T I_3 \end{bmatrix}}_{B} \ddot{\mathbf{c}}_k + \mathrm{w}_{k-1}$$

$$\mathbf{p}_{\mathbf{ZMP},k} = \underbrace{\begin{bmatrix} I_3 & 0_3 & -\frac{z_c}{g} I_3 \end{bmatrix}}_{C} \begin{bmatrix} \mathbf{c} \\ \dot{\mathbf{c}} \\ \ddot{\mathbf{c}} \end{bmatrix}_k + v_k, \tag{13}$$

with

$$\ddot{\mathbf{c}}_k = \frac{\ddot{\mathbf{c}}_k - \ddot{\mathbf{c}}_{k-1}}{T}. \tag{14}$$

Here, k is the time index and $\dot{\mathbf{c}}$ the CoM velocity. The input $\ddot{\mathbf{c}}$ is piecewise constant over the sampling time interval T, i.e. $\ddot{\mathbf{c}}(t) = \ddot{\mathbf{c}}_{kk}, \quad t_k \leq t < t_{k+1} = t_k + T$. w and v are the process and measurements noises, respectively. w and v are assumed to be Gaussian, independent and mutually uncorrelated with zero mean and covariances Q and R, respectively defined as

$$\begin{aligned} E(\mathrm{w}_k) &= E(v_k) = E\left(\mathrm{w}_k v_i^T\right) = 0 \\ Q &= \delta_{ki} E\left(\mathrm{w}_k \mathrm{w}_i^T\right); \; R = \delta_{ki} E\left(v_k v_i^T\right), \\ \delta_{ki} &= \left\{ \begin{array}{ll} 1 & i = k \\ 0 & i \neq k \end{array} \right\}, \end{aligned} \tag{15}$$

where $E(\cdot)$ stands for the expectation of $(\cdot)$.

In general, the CoM frame origin is not necessarily to be the same as the base frame. The CoM may have an offset $\mathbf{c}_{\text{offset}}$ as expressed in O_w. An example of this offset is shown in Fig. 3, the CoM has an x_{offset} from the base frame which has to be considered in the estimation. The IMU output acceleration $\dot{\mathbf{v}}_I$ and angular velocity ω_I are utilized to compute $\ddot{\mathbf{c}}$ in Eq. (14) as

$$\ddot{\mathbf{c}} = A_I^w \dot{\mathbf{v}}_I + A_I^w \omega_I \times \left(A_I^w \omega_I \times (\mathbf{A}_b r_I + \mathbf{c}_{\text{offset}})\right) + A_I^w \dot{\omega}_I \times (\mathbf{A}_b r_I + \mathbf{c}_{\text{offset}}). \tag{16}$$

Then, the model (13) along with Eqs. (14) and (16) are used directly in the stable adaptive KF which is proposed by the author.[69] First, define the states vector $\mathrm{x} = [\, \mathbf{c}^T \; \dot{\mathbf{c}}^T \; \ddot{\mathbf{c}}^T \,]^T$, then a priori estimate of the state vector $\hat{\mathrm{x}}_k^-$ is given by

$$\hat{\mathrm{x}}_k^- = A\, \hat{\mathrm{x}}_{k-1} + B\, \ddot{\mathbf{c}}_k, \tag{17}$$

with a priori estimated covariance P^-

$$P_k^- = A\, P_{k-1}\, A^T + Q_{k-1}. \tag{18}$$

The measurement residual e and its mean $\bar{e}$ are defined as

$$e_k = \mathbf{p}_{\mathbf{ZMP}}^{\mathbf{F_E}} - C\, \hat{\mathrm{x}}_k^-, \tag{19}$$

and

$$\bar{e}_k = \alpha_1\, \bar{e}_{k-1} + \frac{1}{N_R}\, e_k, \tag{20}$$

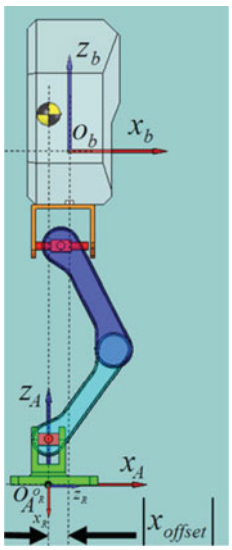

Fig. 3. (Colour online) Base frame offset.

respectively, where N_R is a positive tuning constant and

$$\alpha_1 = \frac{N_R - 1}{N_R}. \tag{21}$$

The measurement noise covariance matrix R is updated as

$$R_k = |\operatorname{diag}(\alpha_1 R_{k-1} + \Delta R_k)|, \tag{22}$$

where diag stands for the diagonal matrix. ΔR is given by

$$\Delta R_k = \frac{1}{N_R - 1}(e_k - \bar{e}_k)(e_k - \bar{e}_k)^T - \frac{1}{N_R}\left(C P^- C^T\right)_k. \tag{23}$$

A posteriori estimate $\hat{\mathrm{x}}$ is obtained using the update rule

$$\hat{\mathrm{x}}_k = \hat{\mathrm{x}}_k^- + K_k e_k, \tag{24}$$

where K is KF gain and expressed by

$$K_k = P_k^- C^T \left(C P_k^- C^T + R_k\right)^{-1}. \tag{25}$$

A posteriori covariance P is updated by

$$P_k = (I - K_k C) P_k^-, \tag{26}$$

where I is the identity matrix. The process covariance matrix Q is updated by the expression

$$Q_k = |\operatorname{diag}(\alpha_2 Q_{k-1} + \Delta Q_k)|, \tag{27}$$

here, ΔQ is defined by

$$\Delta Q_k = \frac{1}{N_Q}\left(P_k - A P_{k-1} A^T\right) + \frac{1}{N_Q - 1}\left(\hat{\Lambda}_k - \bar{\Lambda}_k\right)\left(\hat{\Lambda}_k - \bar{\Lambda}_k\right)^T, \tag{28}$$

where N_Q is a positive tuning constant and

$$\alpha_2 = \frac{N_Q - 1}{N_Q}. \tag{29}$$

$\hat{\Lambda}$ and $\bar{\Lambda}$ are the state error and its mean, respectively. They are defined by

$$\hat{\Lambda}_k = \hat{\mathrm{x}}_k - \hat{\mathrm{x}}_k^-, \tag{30}$$

and

$$\bar{\Lambda}_k = \alpha_2 \bar{\Lambda}_{k-1} + \frac{1}{N_Q} \hat{\Lambda}_k, \tag{31}$$

respectively. For convenience, the time index k is removed later on. Then, the base frame position and velocity are calculated using the estimated states $\hat{\boldsymbol{c}}$ and $\hat{\dot{\boldsymbol{c}}}$ as:

$$\mathbf{p}_b = \hat{\boldsymbol{c}} + \mathbf{c}_{\text{offset}}, \tag{32}$$

and

$$\mathbf{v}_b = \hat{\dot{\boldsymbol{c}}} + A_I^w \omega_I \times \mathbf{c}_{\text{offset}}, \tag{33}$$

respectively.

5. Link Torque Computation

In the proposed approach, the joint friction estimation depends on the knowledge of the applied joint control torque τ and the transmitted torque to the link τ^l. It can be stated mathematically as

$$\begin{pmatrix} \tau_{\mathbf{L}} \\ \tau_{\mathbf{R}} \end{pmatrix} = \begin{pmatrix} \mathbf{u}_{\mathbf{F_L}} \\ \mathbf{u}_{\mathbf{F_R}} \end{pmatrix} + \begin{pmatrix} \tau_{\mathbf{L}}^l \\ \tau_{\mathbf{R}}^l \end{pmatrix}, \tag{34}$$

where $\tau_{\mathbf{L}}^l$ and $\tau_{\mathbf{R}}^l$ are the transmitted torque to the manipulator's left and right leg**s** links, respectively. Referring to Eq. (5), the links torque vector can be represented by the reduced biped model as

$$\begin{pmatrix} \tau_{\mathbf{L}}^l \\ \tau_{\mathbf{R}}^l \end{pmatrix} = \bar{\mathbf{H}} \begin{pmatrix} \dot{\mathbf{v}}_b \\ \dot{\boldsymbol{\omega}}_b \\ \ddot{\boldsymbol{\theta}}_{\mathbf{L}} \\ \ddot{\boldsymbol{\theta}}_{\mathbf{R}} \end{pmatrix} + \begin{pmatrix} \mathbf{b}_{\mathbf{L}} \\ \mathbf{b}_{\mathbf{R}} \end{pmatrix} - \begin{pmatrix} \mathbf{u}_{\mathbf{E_L}} \\ \mathbf{u}_{\mathbf{E_R}} \end{pmatrix}, \tag{35}$$

with

$$\bar{\mathbf{H}} = \begin{pmatrix} H_{31} & H_{32} & H_{33} & 0 \\ H_{41} & H_{42} & 0 & H_{44} \end{pmatrix}. \tag{36}$$

In Eq. (35), the right-hand side is the response due to the vectors $\tau_{\mathbf{L}}^l$ and $\tau_{\mathbf{R}}^l$ from the total applied joint control torque vector. Moreover, Eq. (35) explains that the reaction forces are the net transmitted forces and torques to the robot's links.

The basic idea of the friction estimation is to compute the right-hand side of Eq. (35). The bias term components $\mathbf{b_L}$ and $\mathbf{b_R}$ contain the gravity and Coriolis effects. Hence, the bias term can be formulated as

$$\mathbf{b_m} = \mathbf{f_m}\left(\mathbf{A}_b, \boldsymbol{\theta}_{\mathbf{m}}, \boldsymbol{\omega}_{\mathbf{m}}, \boldsymbol{\omega}_b, \mathbf{v}_b\right). \tag{37}$$

All of the variables required to compute $\mathbf{b_m}$ are known either by direct measurements or estimation explained in Sections 3 and 4.

The effect of the reaction forces $\mathbf{u_{E_m}}$ can be calculated based on the contact force sensors readings $\mathbf{F_{E_R}}$ and $\mathbf{F_{E_L}}$. These forces, $\mathbf{F_{E_m}}$, are mapped to the links by using the Jacobian $\mathbf{J_{F_m}}$ as

$$\mathbf{u_{E_m}} = \mathbf{J^T_{F_m}}(\mathbf{x})\,\mathbf{F_{E_m}}. \tag{38}$$

The Jacobian $\mathbf{J_{F_m}}$ computation depends on the robot geometry which is known. The matrices H_{ij} for $j \in \{1, 2, 3, 4\}$, $i \in \{3, 4\}$ depend on $\boldsymbol{\theta}$ and $\mathbf{A}_b$ only and they are both known. The main difficulty is the existence of the angular acceleration terms which are in most cases unmeasured directly. One solution to this problem is using the band limited periodic excitation trajectories.[70] However, it is not always possible. Another solution is using offline numerical differentiation.[12] However, it is inapplicable in the real time applications. One more solution is using the filtered dynamic model.[71,72] Here, the non-slipping foot constraint is used to calculate the angular accelerations for the DS and SS phases. The acceleration of the foot frame $\ddot{\mathbf{p}}_\mathbf{m}$ can be obtained by double differentiating the position of the foot frame $\mathbf{p_m}$ as

$$\mathbf{J_m}(\mathbf{x}) \begin{bmatrix} \dot{\mathbf{v}}_b \\ \dot{\boldsymbol{\omega}}_b \\ \ddot{\boldsymbol{\theta}}_\mathbf{m} \end{bmatrix} + \dot{\mathbf{J}}_\mathbf{m}(\mathbf{x}) \begin{bmatrix} \mathbf{v}_b \\ \boldsymbol{\omega}_b \\ \dot{\boldsymbol{\theta}}_\mathbf{m} \end{bmatrix} = \ddot{\mathbf{p}}_\mathbf{m}, \tag{39}$$

where $\mathbf{J_m}$ is the Jacobian of the foot frame origin and it can be expressed in terms of its sub-matrices $\mathbf{J_{m_i}}$, $i = 1, 2, 3$ as

$$\mathbf{J_m} = \begin{bmatrix} \mathbf{J_{m_1}} & \mathbf{J_{m_2}} & \mathbf{J_{m_3}} \end{bmatrix}, \tag{40}$$

$\dot{\mathbf{J}}_\mathbf{m}$ is the first derivative of $\mathbf{J_m}$. The base acceleration is measured based on the IMU position and readings, therefore, Eq. (39) can be written as

$$\begin{bmatrix} \mathbf{J_{m_2}} & \mathbf{J_{m_3}} \end{bmatrix} \begin{bmatrix} \dot{\boldsymbol{\omega}}_b \\ \ddot{\boldsymbol{\theta}}_\mathbf{m} \end{bmatrix} = \ddot{\mathbf{p}}_\mathbf{m} - \dot{\mathbf{J}}_\mathbf{m}(\mathbf{x}) \begin{bmatrix} \mathbf{v}_b \\ \boldsymbol{\omega}_b \\ \dot{\boldsymbol{\theta}}_\mathbf{m} \end{bmatrix} - \mathbf{J_{m_1}} \dot{\mathbf{v}}_b. \tag{41}$$

However, the biped has two phases. The formulations for these phases are as follows:

5.1. DS phase

In the DS phase, bearing in mind that there are neither feet accelerations nor slipping, i.e. $\ddot{\mathbf{p}}_\mathbf{L} = \ddot{\mathbf{p}}_\mathbf{R} \simeq 0$, then the angular accelerations can be calculated as

$$\begin{bmatrix} \dot{\boldsymbol{\omega}}_b \\ \ddot{\boldsymbol{\theta}}_\mathbf{L} \\ \ddot{\boldsymbol{\theta}}_\mathbf{R} \end{bmatrix} = \mathbf{J}^T_{DS} \left(\mathbf{J}_{DS} \mathbf{J}^T_{DS} \right)^{-1} \Upsilon_{DS}, \tag{42}$$

where

$$\Upsilon_{DS} = \begin{bmatrix} -\dot{\mathbf{J}}_\mathbf{L}(\mathbf{x}) \begin{bmatrix} \mathbf{v}_b \\ \boldsymbol{\omega}_b \\ \dot{\boldsymbol{\theta}}_\mathbf{L} \end{bmatrix} - \mathbf{J_{L_1}} \dot{\mathbf{v}}_b \\ -\dot{\mathbf{J}}_\mathbf{R}(\mathbf{x}) \begin{bmatrix} \mathbf{v}_b \\ \boldsymbol{\omega}_b \\ \dot{\boldsymbol{\theta}}_\mathbf{R} \end{bmatrix} - \mathbf{J_{R_1}} \dot{\mathbf{v}}_b \end{bmatrix}, \tag{43}$$

and

$$\mathbf{J}_{DS} = \begin{bmatrix} \mathbf{J}_{\mathbf{L}_2} & \mathbf{J}_{\mathbf{L}_3} & 0 \\ \mathbf{J}_{\mathbf{R}_2} & 0 & \mathbf{J}_{\mathbf{R}_3} \end{bmatrix}. \tag{44}$$

This fulfills the requirements to calculate the link torque in Eq. (35). Then the friction is estimated from Eq. (34) as

$$\hat{\mathbf{u}}_{\mathbf{F_m}} = \tau_{\mathbf{m}} - \tau^l_{\mathbf{m}}, \tag{45}$$

where $\hat{\mathbf{u}}_{\mathbf{F}}$ is the estimated joint friction vector.

The estimated link torque can be used in the control loops to compensate for the friction. However for the SS phase, the friction for the swinging leg cannot be estimated using this strategy. For this reason, it is necessary to use models for the friction and identify their parameters while the leg is in contact as in Section 6.

5.2. SS phase

For the SS phase, assuming that there is no foot acceleration nor slipping for the foot which is in contact, i.e. $\ddot{\mathbf{p}}_{\mathbf{m}} \simeq \mathbf{0}$, then the angular accelerations can be calculated from Eq. (41) as

$$\begin{bmatrix} \dot{\boldsymbol{\omega}}_b \\ \ddot{\boldsymbol{\theta}}_{\mathbf{m}} \end{bmatrix} = \mathbf{J}^T_{SS} \left(\mathbf{J}_{SS} \mathbf{J}^T_{SS} \right)^{-1} \Upsilon_{SS}, \tag{46}$$

where

$$\Upsilon_{\mathbf{SS}} = -\dot{\mathbf{J}}_{\mathbf{m}}(\mathbf{x}) \begin{bmatrix} \mathbf{v}_b \\ \boldsymbol{\omega}_b \\ \dot{\boldsymbol{\theta}}_{\mathbf{m}} \end{bmatrix} - \mathbf{J}_{\mathbf{m_1}} \dot{\mathbf{v}}_b, \tag{47}$$

and

$$\mathbf{J}_{SS} = \begin{bmatrix} \mathbf{J}_{\mathbf{m_2}} & \mathbf{J}_{\mathbf{m_3}} \end{bmatrix}. \tag{48}$$

Then the link torque is formulated as

$$\tau^l_{\mathbf{m}} = \bar{\mathbf{H}}_{\mathbf{m}} \begin{pmatrix} \dot{\mathbf{v}}_b \\ \dot{\boldsymbol{\omega}}_b \\ \ddot{\boldsymbol{\theta}}_{\mathbf{m}} \end{pmatrix} + \mathbf{b}_{\mathbf{m}} - \mathbf{u}_{\mathbf{E_m}}, \tag{49}$$

where

$$\bar{\mathbf{H}}_{\mathbf{m}} = \begin{cases} (H_{31} \quad H_{32} \quad H_{33}), \mathbf{m} = \mathbf{L} \\ (H_{41} \quad H_{42} \quad H_{44}), \mathbf{m} = \mathbf{R} \end{cases}.$$

The calculated $\tau^l_{\mathbf{m}}$ is substituted in Eq. (45) to estimate the joint friction vector for the joints of the leg $\mathbf{m}$.

6. Friction Model Parameter Identification

The estimated friction in Eq. (45) depends on the measurement-based strategy and functions only when the foot is in contact with the ground. Therefore, for the swinging leg, a friction model is adopted to represent the frictional forces at the leg joints. The estimated friction in Eq. (45) is used to identify the adopted model parameters. Thus, the model parameters are adaptively identified in

every step the biped walks. Without loss of generality, for the joint n, the friction model is written as a function of the model parameters vector ϕ_n and the input vector ϑ_n as

$$\hat{\mathbf{u}}^n_{\mathbf{F_m}} = f_n\left(\vartheta_n, \phi_n\right), \tag{50}$$

where $f(.)$ can be linear or nonlinear function and $\hat{\mathbf{u}}^n_{\mathbf{F_m}}$ the estimated friction for the joint n. For a number of samples N_s, the least squares (LS) estimate $\hat{\phi}_n$ is

$$\begin{aligned}\hat{\phi}_n &= \min_{\phi_n} \sum_{\mathbf{j}=1}^{N_s} \left(\hat{\mathbf{u}}^n_{\mathbf{F_{m_j}}} - f_{n_\mathbf{j}}\left(\vartheta_{n\mathbf{j}}, \phi_n\right)\right)^2 \\ &= \min_{\phi_n} \left(\underline{\hat{\mathbf{u}}}^n_{\mathbf{F_m}} - \underline{f}_n\left(\underline{\vartheta}_n, \phi_n\right)\right)\left(\underline{\hat{\mathbf{u}}}^n_{\mathbf{F_m}} - \underline{f}_n\left(\underline{\vartheta}_n, \phi_n\right)\right)^T, \end{aligned} \tag{51}$$

where

$$\underline{\hat{\mathbf{u}}}^n_{\mathbf{F_m}} = \begin{bmatrix} \hat{\mathbf{u}}^n_{\mathbf{F_{m_1}}} & \hat{\mathbf{u}}^n_{\mathbf{F_{m_2}}} & \cdots & \hat{\mathbf{u}}^n_{\mathbf{F_{m_{N_s}}}} \end{bmatrix}, \tag{52}$$

and

$$\underline{f}_n\left(\underline{\vartheta}_n, \phi_n\right) = \begin{bmatrix} f_{n_1}\left(\vartheta_{n_1}, \phi_n\right) & f_{n_2}\left(\vartheta_{n_2}, \phi_n\right) & \cdots & f_{n_{\mathbf{N_s}}}\left(\vartheta_{n_{\mathbf{N_s}}}, \phi_n\right) \end{bmatrix}. \tag{53}$$

Equation (50) is for one joint**.** For $\bar{N}$ joints, Eq. (50) can be extended as

$$\hat{\mathbf{u}}_{\mathbf{F_m}} = \mathbf{f_m}\left(\varphi_\mathbf{m}, \Phi_\mathbf{m}\right), \tag{54}$$

where

$$\varphi_\mathbf{m} = \mathrm{diag}\left(\begin{bmatrix} \vartheta_1^T & \cdots & \vartheta_{\bar{N}}^T \end{bmatrix}^T\right),$$

and

$$\Phi = \begin{bmatrix} \phi_1^T & \cdots & \phi_{\bar{N}}^T \end{bmatrix}^T.$$

The goal is to estimate Φ. The vector $\varphi_\mathbf{m}$ is the angular speed of the joints and is indeed known. The friction vector $\hat{\mathbf{u}}_{\mathbf{F_m}}$ is also known from Eq. (45). Then the estimated parameter vector $\hat{\Phi}$ is given by

$$\hat{\Phi}_\mathbf{m} = \arg\min_{\Phi_\mathbf{m}} \frac{1}{2}\left(\hat{\mathbf{u}}_{\mathbf{F_m}} - \mathbf{f_m}\left(\varphi_\mathbf{m}, \Phi_\mathbf{m}\right)\right)\left(\hat{\mathbf{u}}_{\mathbf{F_m}} - \mathbf{f_m}\left(\varphi_\mathbf{m}, \Phi_\mathbf{m}\right)\right)^T. \tag{55}$$

Equation (55) is used when the foot is in contact with the ground. Once the foot loses contact, the joint friction is calculated by employing the estimated model parameters vector $\hat{\Phi}$ into the adopted friction model and then the friction model is used for joint friction compensation.

7. Results

A 12 DOF biped model is used for the simulations. It consists of two legs, each has 6 DOF, and a trunk connecting them. The hip has three joint axes, the ankle has two joints and the knee has one joint (Fig. 4). The dimensions are taken to match our experimental humanoid robot SURALP. The details of contact modeling and simulation algorithm are in ref. [73]. The body frame has an offset $x_{\text{offset}} = 25$ mm.

All measurements and calculations are in the world frame. The IMU is located with a position $r_I = [\,0.01\ -0.01\ 0.02\,]^T$ and attitude $A^I_b = I_3$, where I_3 is a 3×3 identity matrix. In the simulations, the 3-axes IMU which is available in MATLAB Simulink is used. It is composed of 3-axes accelerometer

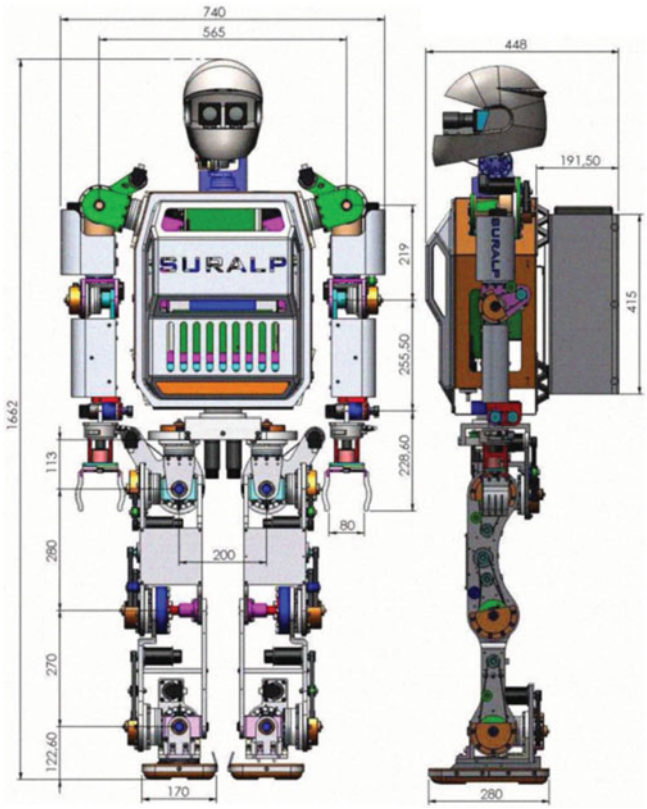

Fig. 4. (Colour online) SURALP dimensions.

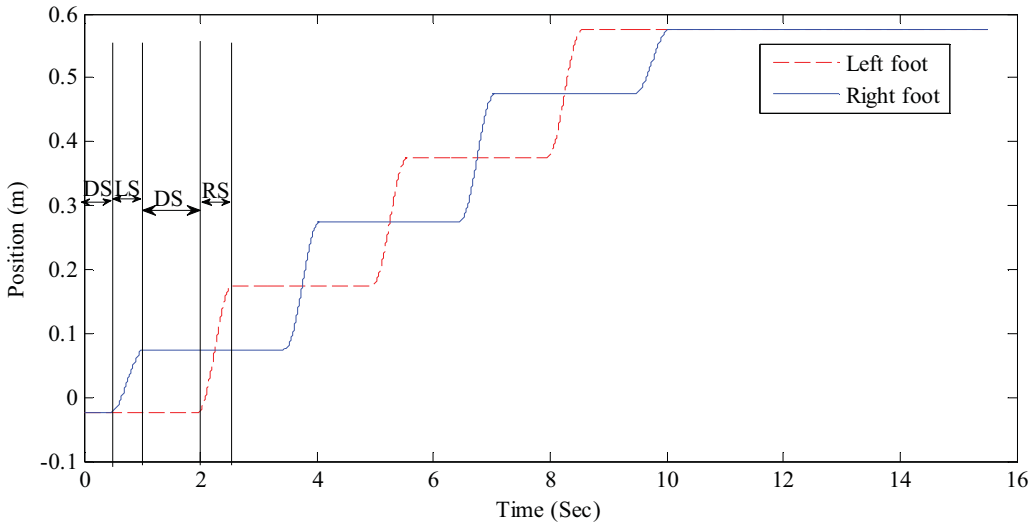

Fig. 5. (Colour online) Foot walking trajectories, DS stands for the double support phase, LS stands for the left leg single support phase, and RS stands for the right leg single support phase.

and 3-axes gyroscope with contaminated noise. Each foot has four force sensors. Each force sensor is 3-axes and located at a known position with respect to the foot frame.[60]

7.1. Walking trajectory

The foot walking trajectories are shown in Fig. 5. The biped has a SS period of 0.6 s and a DS period of 0.9 s. It starts walking after 0.5 s, left single support (LS) then DS then right single support (RS) and so forth. The robot stops at the time instant 10.1 s.

Table I. True friction model parameters for each joint of the leg.

	θ_1	θ_2	θ_3	θ_4	θ_5	θ_6
γ_1	0.7	0.6	0.5	0.4	0.2	0.05
γ_2	100	100	100	100	100	100
γ_3	10	10	10	10	10	10
γ_4	0.6	0.5	0.4	0.3	0.02	0.01
γ_5	100	100	100	100	100	100
γ_6	0.9	0.9	0.9	0.9	0.9	0.9

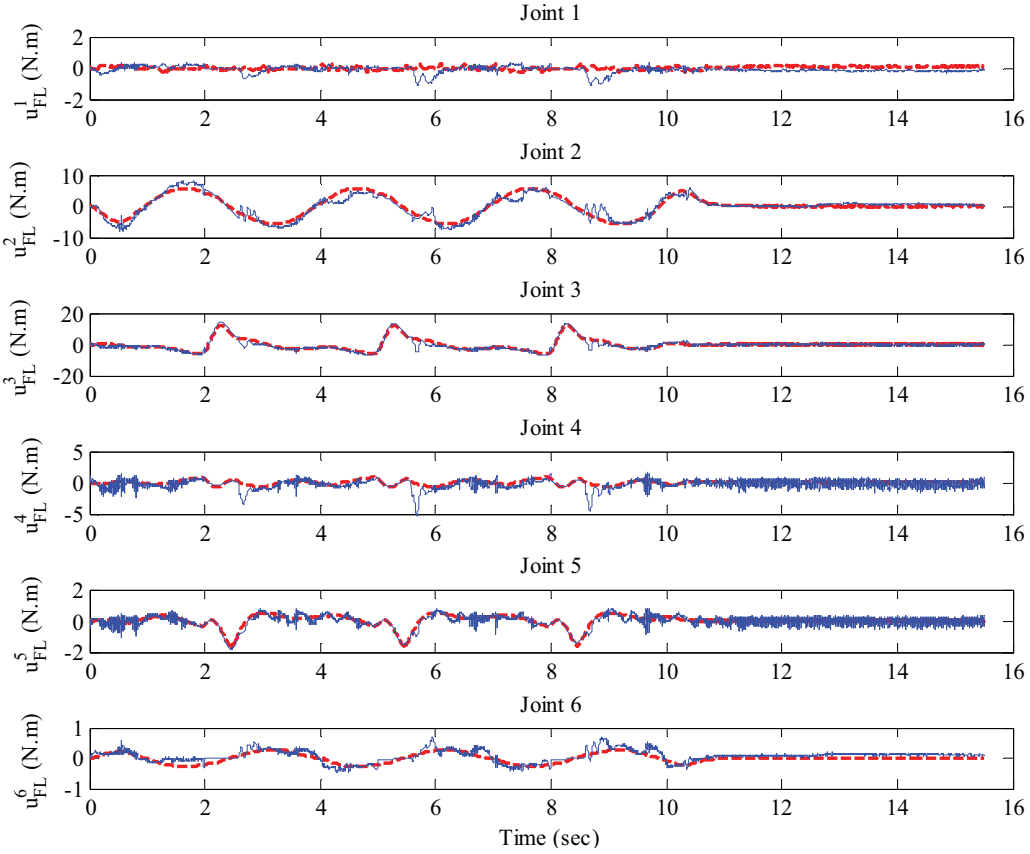

Fig. 6. (Colour online) The estimated joint friction (solid blue line) and the true generated joint friction (dashed red line) for the left leg joints.

Figure 5 shows the negative value of the x_{offset} where both of the feet frames origins are at -0.025 m as shown in Fig. 3 too.

7.2. Joint friction generation

Here, the joint friction is generated using the nonlinear model[21]

$$\mathbf{u_F} = \gamma_1 \left(\tanh\left(\gamma_2 \dot{\boldsymbol{\theta}}\right) - \tanh\left(\gamma_3 \dot{\boldsymbol{\theta}}\right)\right) + \gamma_4 \tanh\left(\gamma_5 \dot{\boldsymbol{\theta}}\right) + \gamma_6 \dot{\boldsymbol{\theta}}, \tag{56}$$

where γ_i, $i = 1, \cdots, 6$ are positive constants. The model has the viscous dissipation term $\gamma_6 \dot{\boldsymbol{\theta}}$ and the coulomb friction term $\gamma_4 \tanh(\gamma_5 \dot{\boldsymbol{\theta}})$. It captures the Stribeck effect by the term $\tanh(\gamma_2 \dot{\boldsymbol{\theta}}) - \tanh(\gamma_3 \dot{\boldsymbol{\theta}})$. The static coefficient of friction can be approximated by $\gamma_1 + \gamma_4$.

The parameters values of the friction model (56) for each joint of the leg are listed in Table I. The corresponding generated true friction is shown Fig. 6 as the dashed red line.

7.3. Joint friction estimation

To be more realistic, Eq. (56) is used solely for the generation of the joint friction. To estimate the friction, another model which differs from Eq. (56) is adopted. Here, the adopted model is linear in its parameters. The coulomb and viscous friction effects are considered. For joint n, the adopted friction model is written as

$$\hat{\mathbf{u}}^{n}_{\mathbf{F_m}} = F^{n}_{c}\,\mathrm{sgn}\left(\dot{\theta}_n\right) + F^{n}_{v}\dot{\theta}_n, \tag{57}$$

where F_v is the viscous friction coefficient and F_c the coulomb friction. When the foot is in contact, the estimated friction $\hat{\mathbf{u}}_{\mathbf{F_m}}$ from Eq. (45) is used to estimate F_v and F_c for each joint. Then, when the leg is swinging, the estimated parameters $\hat{F}_v$ and $\hat{F}_c$ are used to calculate the friction forces for each joint. Equation (57) can be written in a matrix form that includes all the joint friction values for the leg **m** as

$$\hat{\mathbf{u}}_{\mathbf{F_m}} = \varphi^{T}\,\Phi, \tag{58}$$

where

$$\varphi^{T} = \begin{bmatrix} \mathrm{sgn}\left(\dot{\theta}_1\right) & 0 & 0 & \dot{\theta}_1 & 0 & 0 \\ 0 & \ddots & 0 & 0 & \ddots & 0 \\ 0 & 0 & \mathrm{sgn}\left(\dot{\theta}_6\right) & 0 & 0 & \dot{\theta}_6 \end{bmatrix}_{6\times 12}, \tag{59}$$

$$\Phi = \begin{bmatrix} F_c \\ F_v \end{bmatrix}_{12\times 1}, \tag{60}$$

$$F_c = \begin{bmatrix} F^{1}_{c} & F^{2}_{c} & \cdots & F^{6}_{c} \end{bmatrix}^{T}, \tag{61}$$

and

$$F_v = \begin{bmatrix} F^{1}_{v} & F^{2}_{v} & \cdots & F^{6}_{v} \end{bmatrix}^{T}. \tag{62}$$

Then, by storing a number of samples N_s, the estimated parameter vector $\hat{\Phi}$ is calculated by

$$\hat{\Phi} = \left(\sum_{j=1}^{N_s} \varphi\left(j\right)\varphi^{T}\left(j\right)\right)^{-1}\left(\sum_{j=1}^{N_s} \varphi\left(j\right)\hat{\mathbf{u}}_{\mathbf{F_m}}\left(j\right)\right). \tag{63}$$

For real time applications, $\hat{\Phi}$ can be estimated recursively using the recursive least squares method (RLS). The RLS algorithm is

$$\hat{\Phi}_k = \hat{\Phi}_{k-1} + K_{RLS_k} e_{RLS_k}, \tag{64}$$

$$e_{RLS_k} = \hat{\mathbf{u}}_{\mathbf{F_m}} - \varphi^{T}_{k}\hat{\Phi}_{k-1}, \tag{65}$$

$$K_{RLS_k} = P_{RLS_{k-1}}\varphi_k\left(I + \varphi^{T}_{k} P_{RLS_{k-1}}\varphi_k\right)^{-1}, \tag{66}$$

$$P_{RLS,k} = \left(I - K_{RLS,k}\,\varphi^{T}_{k}\right) P_{RLS,k-1}, \tag{67}$$

where the matrix P_{RLS} can be interpreted as the covariance of the parameter vector. The RLS method is used here for the estimation as a real time application. The estimation initializations for the adaptive KF and the RLS algorithm are listed in Table II.

Joint friction is computed simultaneously for all joints. The switching between the DS and the SS phases is time based. The two legs are assumed to have the same frictional models, the same number of joints and the same number of the ground contact points at each foot. The estimation process is

Table II. The adaptive KF and RLS initializations.

Parameter	Value
Q_0	I_9
R_0	$10^{-4} I_3$
N_R	1000
N_Q	5000
$\hat{\mathbf{x}}_0$	$0_{9\times 1}$
P_0	$10 I_9$
$\bar{e}_0$	$0_{3\times 1}$
$\bar{\Lambda}_0$	$0_{9\times 1}$
Φ_0	$0_{12\times 1}$
P_{RLS_0}	$10 I_{12}$

as follows: in the DS phase, the friction compensation is model free and the friction is estimated based on the force measurements. At the same time, the estimated friction is used to identify the friction model parameters F_v and F_c for each joint in each leg. At the time instant $t = 0.5$ s, the robot switches from the DS phase to the LS phase. At this instant, the friction models with the identified parameters $\hat{F}_v$ and $\hat{F}_c$ are used to compute the friction for the right leg joints. For the left leg joints, the friction estimation is still model-free and the corresponding friction model parameters are still being identified. At the time instant $t = 1.1$ s, the robot again switches to the DS phase. Again, the friction estimation is model-free and the friction model parameters are being identified for both legs joints. Hence, the friction model parameters are adaptively identified and corrected. At the time instant $t = 2$ s, the robot switches from the DS phase to the RS phase. At this instant, the friction models with the identified parameters are used to compute the friction for the left leg joints. For the right leg, the friction estimation is still carried on as friction model-free. The corresponding friction model parameters are still being identified, and so forth.

The Estimated friction values for the left leg joints are shown in Fig. 6 (solid blue line). The same goes for the right leg. When the foot is in contact with the ground, the measurement-based online friction compensation is used. When the leg is swinging, the model (57) is used to estimate the joint friction. As depicted in Fig. 6, the estimated joint friction tracks the true friction for all of the friction cases. One observation is that when the foot is in contact, the estimated friction is noisy. This is due to the measured noisy forces. However, when the leg is swinging i.e. when the friction model is used, the friction is much smoother. In these simulations, small and large frictional forces are used to test the ability of the proposed method.

7.4. Joint friction compensation using the FBSE method

To compensate for the joint friction, the control structure in Fig. 7 is used. The position controller is a PD controller with proportional gain $k_p = \text{diag}([\,6\ 2\ 2\ 3\ 3\ 6\,] \times 10^3)$ and derivative gain $k_d = I_{12}$. The output of the PD controller $\boldsymbol{\tau}_{\text{pos}}$ is

$$\boldsymbol{\tau}_{\text{pos}} = \begin{bmatrix} k_p & 0 \\ 0 & k_p \end{bmatrix} \left(\boldsymbol{\theta}^{\text{ref}} - \boldsymbol{\theta}\right) + k_d \left(\dot{\boldsymbol{\theta}}^{\text{ref}} - \dot{\boldsymbol{\theta}}\right), \tag{68}$$

where $\boldsymbol{\theta}^{\text{ref}}$ and $\dot{\boldsymbol{\theta}}^{\text{ref}}$ are the reference trajectories. Note that $\boldsymbol{\theta}^{\text{ref}}$ is generated based on the desired CoM position $\mathbf{c}^{\text{des}}$. Therefore, the actual $\mathbf{c}$ is compared with $\mathbf{c}^{\text{des}}$. The torque controller output $\boldsymbol{\tau}_{\text{tor}}$ is

$$\boldsymbol{\tau}_{\text{tor}} = \begin{bmatrix} k_{\text{i}} & 0 \\ 0 & k_{\text{i}} \end{bmatrix} \int_0^t \left(\boldsymbol{\tau}_{\text{pos}} - (\boldsymbol{\tau} - \hat{\mathbf{u}}_{\mathbf{F}})\right) d\tau, \tag{69}$$

where k_{i} is the integral gain with vales $k_{\text{i}} = \text{diag}([\,2\ 2\ 1\ 2\ 2\ 4\,])$, τ the integration variable.

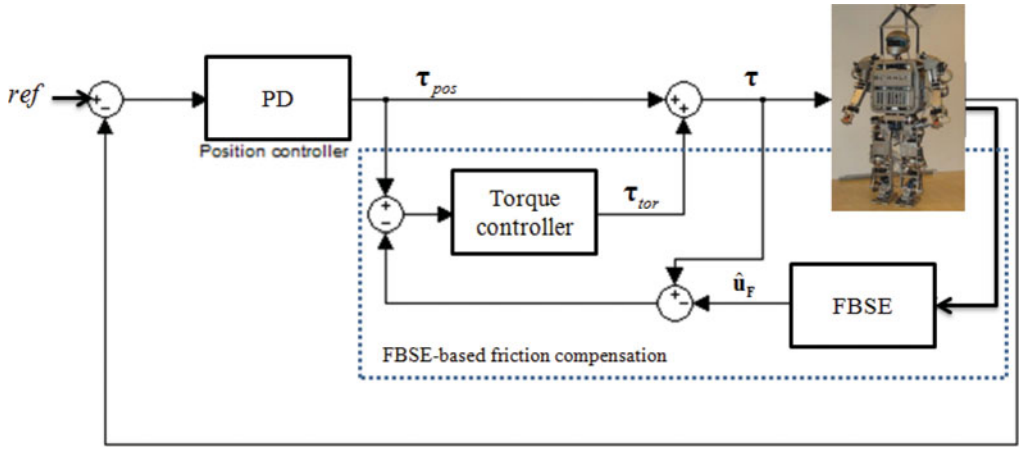

Fig. 7. (Colour online) Friction compensation using the proposed FBSE method.

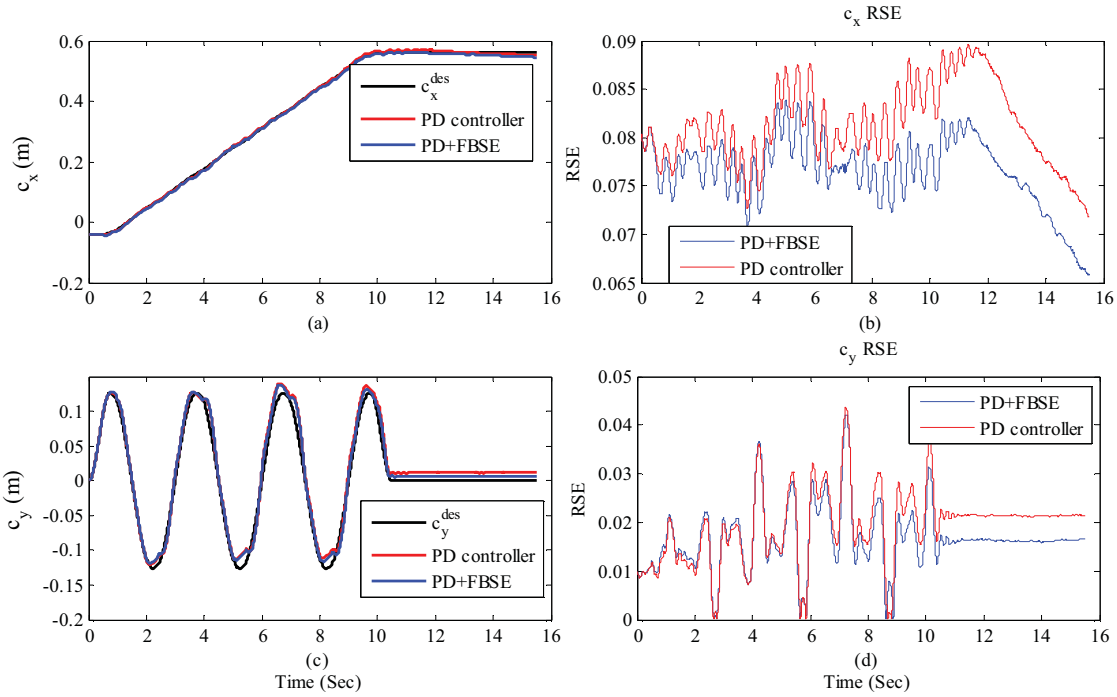

Fig. 8. (Colour online) (a) CoM trajectory in the $x-$ direction c_x, (b) RSE in c_x, (c) CoM trajectory in the $y-$ direction c_y and (d) RSE in c_y.

The root square error (RSE) is used as a performance measure of the response. The RSE is defined by

$$RSE = \sqrt{\left(\mathbf{c}^{\text{des}} - \mathbf{c}\right)^2}. \tag{70}$$

Figure 8 demonstrates the improvement due to the proposed method. First, the conventional PD controller is used alone and its response is compared with the response of the proposed FBSE method. As shown in Fig. 8(b) and (d), the position error of the PD controller alone is higher than the position error when the PD controller is combined with the FBSE method.

8. Conclusion

A Novel FBSE method for estimating the joint friction of walking bipeds is proposed. The method utilizes the readings of IMU and feet contact reaction forces into a reduced model of the biped. The

FBSE method combines the measurement-based strategy with the adaptive model-based methodology to estimate the joint friction. The measurement-based estimation is used when the foot is in contact with ground, while the adaptive model-based friction is used when the leg is swinging. To achieve this estimation, the joint angular accelerations are estimated online using the foot contact non-slipping constraint. Furthermore, the base velocity vector is estimated too by fusing the IMU readings and force measurements through the LIPM. Thus the FBSE method requires the IMU, joint encoders and ground contact force measurements. The FBSE does not require excessive joint torque sensors. The results show that the estimated friction tracks the true one. Furthermore, using the FBSE method in the feedback torque signal improves the response. Although, the method is proposed for bipeds, it can be extended to multi-leg robots easily.

References

1. H. Hirukawa, "Walking biped humanoids that perform manual labour," *Phil. Trans. A Math. Phys. Eng. Sci.* **365**, 65–77 (Jan. 15, 2007).
2. T. Nishiyama, H. Hoshino, K. Sawada, A. Baba, T. Sekine, W. Yamada, A. Terasawa, R. Nakajima, Y. Tokunaga and M. Yoneda, "Communication Agent Embedded in Humanoid Robot," *SICE Annual Conference* (2003), vol. 2, pp. 1514–1519.
3. M. H. Raibert and E. R. Tello, "Legged robots that balance," *IEEE Expert* **1**, 89–89 (1986).
4. M. Koeda, Y. Uda, S. Sugiyama and T. Yoshikawa, "Shuffle Turn and Translation of Humanoid Robots," *IEEE International Conference on Robotics and Automation (ICRA)*, (2011) pp. 593–598.
5. K. Miura, S. Nakaoka, M. Morisawa, F. Kanehiro, K. Harada and S. Kajita, "Analysis on a Friction based "Twirl" for Biped Robots," *IEEE International Conference on Robotics and Automation (ICRA)*, (2010) pp. 4249–4255.
6. S. Kajita, M. Morisawa, K. Miura, S. Nakaoka, K. Harada, K. Kaneko, F. Kanehiro and K. Yokoi, "Biped Walking Stabilization based on Linear Inverted Pendulum Tracking," *IEEE/RSJ International Conference on Intelligent Robots and Systems (IROS)*, (2010) pp. 4489–4496.
7. T. Liu, Y. Inoue and K. Shibata, "A wearable ground reaction force sensor system and its application to the measurement of extrinsic gait variability," *Sensors* **10**, 10240–10255 (2010).
8. U. Seven, T. Akbas, K. Fidan and K. Erbatur, "Bipedal robot walking control on inclined planes by fuzzy reference trajectory modification," *Soft Computing*, **16**(11), 1959–1976 (2012).
9. S.-J. Yi, B.-T. Zhang, D. Hong and D. D. Lee, "Practical Bipedal Walking Control on Uneven Terrain using Surface Learning and Push Recovery," *IEEE/RSJ International Conference on Intelligent Robots and Systems (IROS)*, (2011), pp. 3963–3968.
10. K. Yeoun-Jae, L. Joon-Yong and L. Ju-Jang, "A Balance Control Strategy of a Walking Biped Robot in An Externally Applied Force," *International Conference on Information and Automation (ICIA)*, (2012), pp. 572–577.
11. J. P. Ferreira, M. M. Crisostomo and A. P. Coimbra, "Human gait acquisition and characterization," *IEEE Trans. Instrum. Meas.* **58**, 2979–2988 (2009).
12. B. Siciliano and O. Khatib, *Springer Handbook of Robotics* (Springer-Verlag New York, Inc., 2007).
13. R. H. Hensen, M. Van de Molengraft and M. Steinbuch, "Friction induced hunting limit cycles: A comparison between the LuGre and switch friction model," *Automatica* **39**, 2131–2137 (2003).
14. R. H. Hensen and M. J. van de Molengraft, "Friction Induced Hunting Limit Cycles: An Event Mapping Approach," *Proceedings of the American Control Conference*, (2002) pp. 2267–2272.
15. H. Olsson and K. J. Astrom, "Friction generated limit cycles," *IEEE Trans. Control Syst. Technol.* **9**, 629–636 (2001).
16. B. Bona and M. Indri, "Friction Compensation in Robotics: An Overview," *IEEE European Control Conference on Decision and Control*, (2005) pp. 4360–4367.
17. F. Jatta, R. Adamini, A. Visioli and G. Legnani, "Hybrid Force/Velocity Robot Contour Tracking: An Experimental Analysis of Friction Compensation Strategies," *IEEE International Conference on Robotics and Automation*, (2002), vol. 2, pp. 1723–1728.
18. B. Armstrong-Hélouvry, P. Dupont and C. C. De Wit, "A survey of models, analysis tools and compensation methods for the control of machines with friction," *Automatica* **30**, 1083–1138 (1994).
19. R. H. A. Hellsen, G. Z. Angelis, M. J. G. van de Molengraft, A. G. de Jager and J. J. Kok, "Grey-box modeling of friction: An experimental case-study," *Eur. J. Control* **6**, 258–267 (2000).
20. V. Lampaert, J. Swevers and F. Al-Bender, "Modification of the leuven integrated friction model structure," *IEEE Trans. Autom. Control* **47**, 683–687 (2002).
21. C. Makkar, W. E. Dixon, W. G. Sawyer and G. Hu, "A New Continuously Differentiable Friction Model for Control Systems Design," *Proceedings of IEEE/ASME International Conference on Advanced Intelligent Mechatronics*, (2005) pp. 600–605.
22. K. Joohyung, K. Hoseong, L. Heekuk, S. Keehong, L. Bokman, L. Minhyung, L. Jusuk and R. Kyungsik, "Balancing Control of a Biped Robot," *IEEE International Conference on Systems, Man, and Cybernetics (SMC)*, (2012) pp. 2756–2761.

23. W. Shang, S. Cong and Y. Zhang, "Nonlinear friction compensation of a 2-DOF planar parallel manipulator," *Mechatronics* **18**, 340–346 (2008).
24. R. H. A. Hensen, M. J. G. Van de Molengraft and M. Steinbuch, "Frequency domain identification of dynamic friction model parameters," *IEEE Trans. Control Syst. Technol.* **10**, 191–196 (2002).
25. J. Moreno and R. Kelly, "Manipulator Velocity Field Control with Dynamic Friction Compensation," *IEEE Conference on Decision and Control*, (2003), vol. 4, pp. 3834–3839.
26. J. Moreno, R. Kelly and R. Campa, "Manipulator velocity control using friction compensation," *IEE Proc.-Control Theory Appl.* **150**, 119–126 (2003).
27. D. Kostic, B. de Jager, M. Steinbuch and R. Hensen, "Modeling and identification for high-performance robot control: An RRR-robotic arm case study," *IEEE Trans. Control Syst. Technol.* **12**, 904–919 (2004).
28. G. Morel, K. Iagnemma and S. Dubowsky, "The precise control of manipulators with high joint-friction using base force/torque sensing," *Automatica* **36**, 931–941 (2000).
29. S. Grami and Y. Gharbia, "GMS Friction Compensation in Robot Manipulator," *Conference of the IEEE on Industrial Electronics Society (IECON)*, (2013) pp. 3555–3560.
30. Z. Dongdong, N. Jing, R. Xuemei, G. Herrmann and S. Longo, "Adaptive Control of Robotic Servo System with Friction Compensation," *IEEE Conference on Robotics, Automation and Mechatronics (RAM)*, (2011) pp. 285–290.
31. L. R. Ray, A. Ramasubramanian and J. Townsend, "Adaptive friction compensation using extended Kalman–Bucy filter friction estimation," *Control Eng. Pract.* **9**, 169–179 (2001).
32. P. Vedagarbha, D. M. Dawson and M. Feemster, "Tracking control of mechanical systems in the presence of nonlinear dynamic friction effects," *IEEE Trans. Control Syst. Technol.* **7**, 446–456 (1999).
33. B. Friedland and Y. J. Park, "On adaptive friction compensation," *IEEE Trans. Autom. Control* **37**, 1609–1612 (1992).
34. D. Vischer and O. Khatib, "Design and development of high-performance torque-controlled joints," *IEEE Trans. Robot. Autom.* **11**, 537–544 (1995).
35. L. E. Pfeffer, O. Khatib and J. Hake, "Joint torque sensory feedback in the control of a PUMA manipulator," *IEEE Trans. Robot. Autom.* **5**, 418–425 (1989).
36. A. Mohammadi, M. Tavakoli, H. J. Marquez and F. Hashemzadeh, "Nonlinear disturbance observer design for robotic manipulators," *Control Eng. Pract.* **21**, 253–267 (2013).
37. C. Wen-Hua, D. J. Ballance, P. J. Gawthrop and J. O'Reilly, "A nonlinear disturbance observer for robotic manipulators," *IEEE Trans. Ind. Electron.* **47**, 932–938 (2000).
38. D. Xing, J. Su, Y. Liu and J. Zhong, "Robust approach for humanoid joint control based on a disturbance observer," *Control Theory & Appl. IET* **5**, 1630–1636 (2011).
39. J.-H. Ryu, J. Song and D.-S. Kwon, "A nonlinear friction compensation method using adaptive control and its practical application to an in-parallel actuated 6-DOF manipulator," *Control Eng. Pract.* **9**, 159–167 (2001).
40. B. Armstrong, D. Neevel and T. Kusik, "New results in NPID control: Tracking, integral control, friction compensation and experimental results," *IEEE Trans. Control Syst. Technol.* **9**, 399–406 (2001).
41. V. Lampaert, J. Swevers and F. Al-Bender, "Comparison of Model and Non-Model based Friction Compensation Techniques in the Neighbourhood of Pre-Sliding Friction," *Proceedings of the American Control Conference*, (2004), vol. 2, pp. 1121–1126.
42. S. N. Huang, K. K. Tan and T. H. Lee, "Adaptive friction compensation using neural network approximations," *IEEE Trans. Syst. Man Cybern. C* **30**, 551–557 (2000).
43. V. Vitiello and A. Tornambe, "Adaptive Compensation of Modeled Friction using a RBF Neural Network Approximation," *IEEE Conference on Decision and Control*, (2007) pp. 4699–4704.
44. Y. H. Kim and F. L. Lewis, "Reinforcement Adaptive Learning Neural Network based Friction Compensation for High Speed and Precision," *Proceedings of the IEEE Conference on Decision and Control*, (1998), vol. 1, pp. 1064–1069.
45. G. L. Wang, Y. F. Li and D. X. Bi, "Support vector networks in adaptive friction compensation," *IEEE Trans. Neural Netw.* **18**, 1209–1219 (2007).
46. Y. F. Wang, D. H. Wang and T. Y. Chai, "Modeling and control compensation of nonlinear friction using adaptive fuzzy systems," *Mech. Syst. Signal Process.* **23**, 2445–2457 (2009).
47. L. Mostefai, M. Denai, S. Oh and Y. Hori, "Optimal control design for robust fuzzy friction compensation in a robot joint," *IEEE Trans. Ind. Electron.* **56**, 3832–3839 (2009).
48. W. Yongfu, W. Dianhui and C. Tianyou, "Extraction and adaptation of fuzzy rules for friction modeling and control compensation," *IEEE Trans. Fuzzy Syst.* **19**, 682–693 (2011).
49. D. Velez-Diaz and T. Yu, "Adaptive robust fuzzy control of nonlinear systems," *IEEE Trans. Syst. Man Cybern. B* **34**, 1596–1601 (2004).
50. M. A. Llama, R. Kelly and V. Santibanez, "Stable computed-torque control of robot manipulators via fuzzy self-tuning," *IEEE Trans. Syst. Man Cybern. B* **30**, 143–150 (2000).
51. K. Shiev, N. Shakev, A. V. Topalov and S. Ahmed, "Trajectory Control of Manipulators using Type-2 Fuzzy Neural Friction and Disturbance Compensator," *IEEE International Conference Intelligent Systems (IS)*, (2012) pp. 324–329.
52. R. J. Patton, D. Putra and S. Klinkhieo, "Friction compensation as a fault-tolerant control problem," *Int. J. Syst. Sci.* **41**, 987–1001 (2010).

53. H. Yan, B. Vanderborght, R. Van Ham, W. Qining, M. Van Damme, X. Guangming and D. Lefeber, "Step length and velocity control of a dynamic bipedal walking robot with adaptable compliant joints," *IEEE/ASME Trans. Mechatronics* **18**, 598–611 (2013).
54. P. van Zutven, D. Kostic and H. Nijmeijer, "Foot Placement for Planar Bipeds with Point Feet," *IEEE International Conference on Robotics and Automation (ICRA)*, (2012) pp. 983–988.
55. T. Hase, H. Qingjiu and C. Xuedong, "Performance Analysis of Biped Walking Robot with Circular Feet using Optimal Trajectory Planning Method," *IEEE International Conference on Robotics and Biomimetics*, (2009), pp. 143–148.
56. K. Miyahara, Y. Harada, D. N. Nenchev and D. Sato, "Three-Dimensional Limit Cycle Walking with Joint Actuation," *IEEE/RSJ International Conference on Intelligent Robots and Systems (IROS)*, (2009) pp. 4445–4450.
57. T. Yoshikawa and O. Khatib, "Compliant Humanoid Robot Control by the Torque Transformer," *IEEE/RSJ International Conference on Intelligent Robots and Systems (IROS)*, (2009) pp. 3011–3018.
58. S. I. Han and K. S. Lee, "Robust friction state observer and recurrent fuzzy neural network design for dynamic friction compensation with backstepping control," *Mechatronics* **20**, 384–401 (2010).
59. S. Kajita and K. Tani, "Study of Dynamic Biped Locomotion on Rugged Terrain-Derivation and Application of the Linear Inverted Pendulum Mode," *Proceedings of IEEE International Conference on Robotics and Automation*, (1991), vol. 2, pp. 1405–1411.
60. K. Erbatur, U. Seven, E. Taskiran, O. Koca, M. Yilmaz, M. Unel, G. Kiziltas, A. Sabanovic and A. Onat, "SURALP: A New Full-Body Humanoid Robot Platform," *IEEE-Rsj International Conference on Intelligent Robots and Systems*, (New York, 2009) pp. 4949–4954.
61. I. Hashlamon and K. Erbatur, "Experimental Verification of an Orientation Estimation Technique for Autonomous Robotic Platforms." *Master degree Thesis* (Istanbul: Sabanci University, 2010).
62. K. Erbatur and U. Seven, "Humanoid Gait Synthesis with Moving Single Support ZMP Trajectories," *Proceedings of the 13th Iasted International Conference on Robotics and Applications/Proceedings of the Iasted International Conference on Telematics*, (K. Schilling, ed.) (Anaheim: Acta Press Anaheim, 2007) pp. 95–100.
63. H. Hirukawa, S. Hattori, K. Harada, S. Kajita, K. Kaneko, F. Kanehiro, K. Fujiwara and M. Morisawa, "A Universal Stability Criterion of the Foot Contact of Legged Robots - Adios ZMP," *Proceedings of the IEEE International Conference on Robotics and Automation*, (2006) pp. 1976–1983.
64. K. Erbatur and O. Kurt, "Natural ZMP trajectories for biped robot reference generation," *IEEE Trans. Ind. Electron.* **56**, 835–845 (Mar. 2009).
65. I. Hur, Y. Matsuki, N. Tomokuni, J. Huang and T. Yabuta, "Standing Stability of Surfing Robot without Force Sensor," *25th Annual Conference of the Robotics Society of Japan, 3H11*, (2007) pp. 15–18.
66. S. Kajita, F. Kanehiro, K. Kaneko, K. Fujiwara, K. Harada, K. Yokoi and H. Hirukawa, "Biped Walking Pattern Generation by using Preview Control of Zero-Moment Point," *Proceedings of IEEE International Conference on Robotics and Automation ICRA*, (2003), vol. 2, pp. 1620–1626.
67. B. J. Stephens, "State Estimation for Force-Controlled Humanoid Balance using Simple Models in the Presence of Modeling Error," *IEEE International Conference on Robotics and Automation*, (2011) pp. 3994–3999.
68. I. Hashlamon and K. Erbatur, "Center of Mass States and Disturbance Estimation for a Walking Biped," *IEEE International Conference on Mechatronics, ICM 2013*, Vicenza (ITALY). (2013) pp. 248–253.
69. I. Hashlamon and K. Erbatur, "An improved real-time adaptive Kalman filter with recursive noise covariance updating rules," *Turk. J. Electr. Eng. Comput. Sci.*, Accepted, (2013) doi: 10.3906/elk-1309-60.
70. J. Swevers, C. Ganseman, D. B. Tukel, J. De Schutter and H. Van Brussel, "Optimal robot excitation and identification," *IEEE Trans. Robot. Autom.* **13**, 730–740 (1997).
71. P. Hsu, M. Bodson, S. Sastry and B. Paden, "Adaptive Identification and Control for Manipulators without Using Joint Accelerations," *Proceedings IEEE International Conference on Robotics and Automation*, (1987) pp. 1210–1215.
72. M. Van Damme, P. Beyl, B. Vanderborght, V. Grosu, R. Van Ham, I. Vanderniepen, A. Matthys and D. Lefeber, "Estimating Robot End-Effector Force from Noisy Actuator Torque Measurements," *IEEE International Conference on Robotics and Automation (ICRA)*, (2011) pp. 1108–1113.
73. K. Erbatur and A. Kawamura, "A New Penalty based Contact Modeling and Dynamics Simulation Method as Applied to Biped Walking Robots," *Proceedings of the FIRA World Congress*, Vienna, Austria, (2003).